ELSEVIER

Polymer 42 (2001) 8947–8958

polymer

www.elsevier.com/locate/polymer

New approaches using MW-sensitive detectors in GPC–TREF for polyolefin characterization

Wallace W. Yau*, David Gillespie[1]

Chevron Chemical Company, LLC, 1862 Kingwood Drive, Kingwood, TX 77339, USA

Received 7 March 2001; received in revised form 2 April 2001; accepted 2 April 2001

Abstract

For in-depth analyses of polyolefin microstructures, we have installed the MW-specific light scattering (LS) and viscosity detectors into a home-built hybrid GPC–TREF instrument. Data processing capabilities were developed for this triple-detector system to determine (1) polymer long chain branching (LCB) distribution across the GPC-determined molecular weight distribution (MWD) curve, (2) the GPC-M_z and higher-order MW averages with greatly improved precision to complement the rheological results, and (3) the dependence of polymer MW across the TREF-determined short chain branching (SCB) distribution curve. A 'polymer microstructure plot' is created from the combined overlays of triple-detector GPC–TREF chromatograms to provide a quick view of detecting subtle sample differences in polymer MW, MWD, SCB or LCB. These results can do much more than the use of only the MI and density values for product development or trouble shooting of polymer end-use properties.

Keywords: Polyolefin; GPC-TREF; Branching

1. Introduction

Polyolefin technology has made remarkable progresses in the last four decades [1–6]. New resins are produced to meet the requirement of the high-speed fabrication equipment and the market expansion into high-tech applications. This progress requires strong polymer characterization support to analyze polymer microstructure. To this end, high temperature gel permeation chromatography (GPC or SEC [7]) and temperature rising elution fractionation (TREF [8,9]) have been developed for polyolefin characterization. We have added triple detectors (concentration, RI or IR; viscosity, DP; and light scattering, LS) to the systems to give the much more powerful 3D-GPC (or TriSEC) and 3D-TREF capabilities of studying polyolefin structures.

The 3D-GPC technique separates molecules by their sizes and can be used to measure polymer molecular weight distribution (MWD) and long chain branching (LCB). Using the 3D-GPC instrument, we have developed a GPC-LS method that can determine the high-order MW averages with sufficient precision for studying polymer rheology and MWD relationships. The 3D-TREF technique separates molecules by their melt-dissolution temperatures and can be used to study short chain branching (SCB) and co-monomer composition distribution (CCD) in polyolefins. These molecular structural parameters are of key importance to the performance of polyolefin resins in terms of end-use properties and processing flexibility. By combining the 3D-GPC and 3D-TREF results, we have also created a very useful 'polymer microstructure plot' that can provide a quick detection of subtle molecular structural differences in polymer samples.

2. Experimental

The rheology work was performed using a Rheoscience ARES parallel plate rheometer using 25 mm plates with a 1.5 mm gap at 190°C under nitrogen purge. The zero-shear viscosity was calculated using the Carreau model. The conventional chromatography (GPC) was completed on a Waters Corporation 150C High Temperature Chromatograph equipped with an internal refractometer (RI). The 4-chromatography column set was obtained from Polymer

* Corresponding author. Present address: Equistar Chemicals, LP, Equistar Technology Center, 11530 Northlake Drive, Cincinnati, OH 45249, USA. Tel.: +1-513-530-4368/979-458-0666; fax: +1-513-530-4267/979-862-3989.

E-mail address: wallace.yau@equistarchem.com (W.W. Yau).

[1] Present address: Dow Chemical Co., Freeport, TX 77541, USA.
E-mail address: dgillespie@dow.com (D. Gillespie).

0032-3861/01/$ - see front matter
PII: S0032-3861(01)00392-5

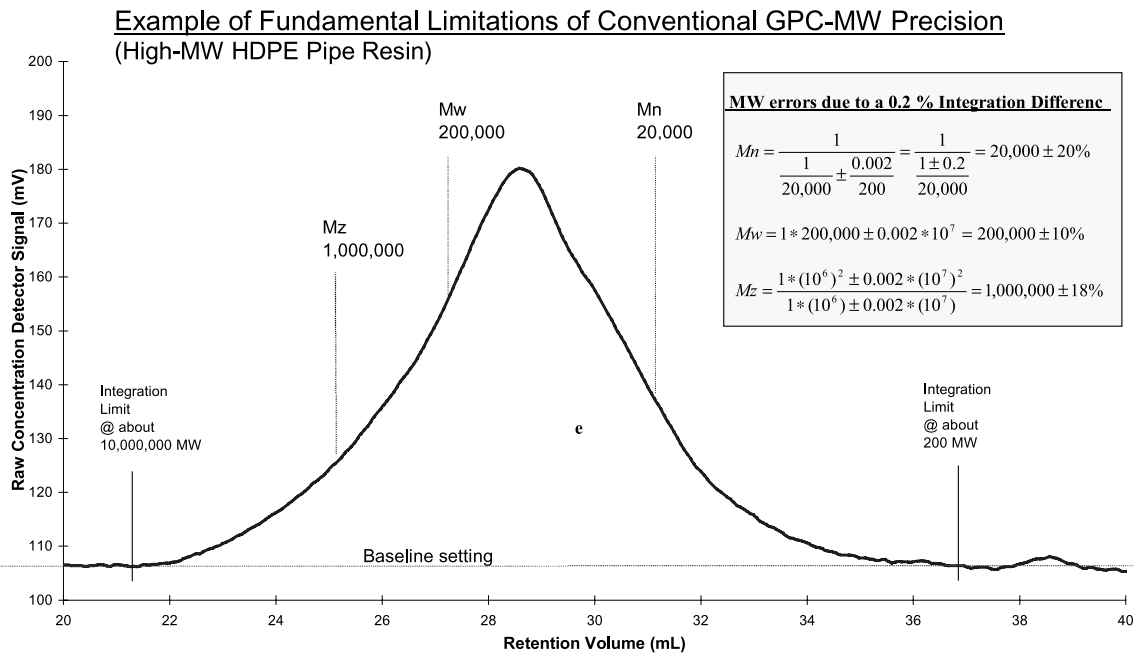

Fig. 1. Fundamental limitation of conventional GPC-MW precision.

Laboratories. The solvent used was 1,2,4-trichlorobenzene (TCB). Concentrations were 2.0 mg/ml, the injection volume was 500 μl, and the flow rate was 0.5 ml/min. Data was collected and processed with Viscotek TriSEC GPC Software version 3.0. The 3D-GPC instrument used an LS detector from Precision Detectors coupled with a viscometer from Viscotek [10], along with the Waters refractometer to make the triple-detector capability. Molecular weight data could then be directly calculated via the LS chromatogram; and the intrinsic viscosity could be calculated via the on-line viscometer. By plotting the intrinsic viscosity as a function of molecular weight, LCB structural information can be obtained in the form of a Mark–Houwink (M–H) plot [11]. The TREF results were obtained on a homemade automated 3D-TREF system [12], the details of which is described in Section 5.

3. High precision M_z by GPC-LS

The successful link between GPC and polymer rheological properties is not very easily attainable. This is because of the limited precision of polymer M_z and higher-order MW averages that are obtainable by GPC. To improve this situation, we propose to increase the precision of these high order MW averages with a new calculation algorithm that uses only the LS elution curve profile, in contrast to conventional GPC using the RI elution curve.

3.1. Background

It is commonly accepted that there is an empirical relationship of the zero-shear viscosity of polymer melt [$\eta(0)$] having a 3.4 power dependency on polymer weight-average molecular weight (M_w):

$$\eta(0) \propto M_w^{3.4} \tag{1}$$

The $\eta(0)$ measurement is sensitive to the entanglement of high molecular weight components in a polymer sample. Polymer melt viscosity is a complex, average property of the polymer MWD. It would be of a great value if the GPC measurement of MWD were able to overlap with this rheology measurement to provide a better understanding of the polymer structure property relationship.

The past attempts of trying to link GPC and rheology have largely been unsuccessful. The precision level required of GPC for such study far exceeds the capability of conventional GPC method using only a concentration detector, e.g. a differential refractometer (RI). Because of the 3.4 power dependence in Eq. (1), an experimental variance of the M_w values at 5, 10, or 20% level in conventional GPC is magnified many times to an unacceptable level for predicting polymer low-shear melt viscosity [13–15].

The precision of conventional GPC for high order MW averages is very much limited by the difficulty of achieving good reproducible settings of baseline and integration limits for MW calculations. This problem is explained by the example shown in Fig. 1. For this GPC elution curve of a high-density polyethylene (HDPE) sample, we processed the same GPC data in two separate times, but purposely used a slightly different baseline and integration at about a slight error of ±0.2% of peak area. A small variance of this magnitude can already cause up to 10% error in M_w and near 20% errors in M_n and M_z (see the inserts in Fig. 1 for

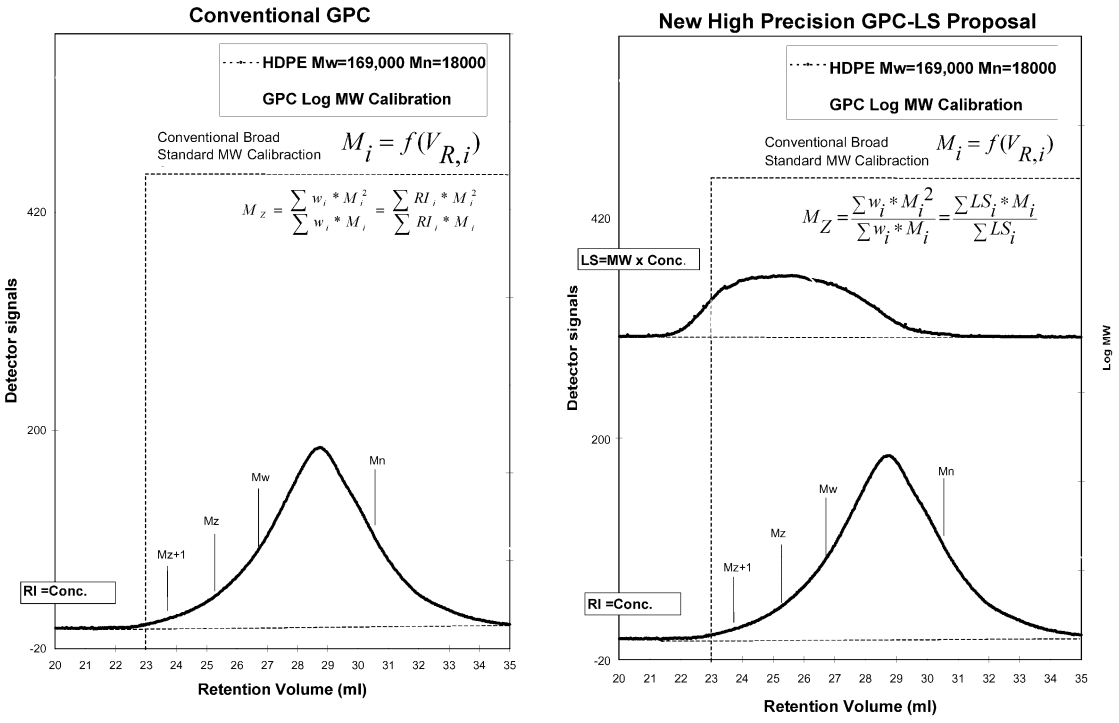

Fig. 2. The contrast of new GPC-LS approach versus conventional GPC.

calculation detail). This goes to show the baseline cutting problem in GPC and how this error can put a limit to precision in conventional GPC, even under good experimental conditions. This precision problem of GPC is worse for higher-order MW averages that are even more sensitive to the high-MW tail of MWD curve. For studying polymer rheology, a much higher precision of GPC-M_z and M_{z+1} values is needed.

Conventional method of using LS detector with GPC (GPC-LS) does not provide the solution to this GPC precision problem. In fact, the precision of the conventional GPC-LS method is even worse than conventional GPC. In conventional GPC-LS, the MW value at each GPC slice needs be calculated as the ratio of the LS signal divided by the RI signal. As sample concentrations become lower and lower when elution approaches the very high-MW regions, the RI signal decreases steadily at a rate faster than the LS signal (Fig. 2). When the RI signal approaches zero and becomes indiscernible with baseline noise, the error in MW calculation by LS/RI ratio for each GPC slice increases dramatically at the high-MW end. There are regions where RI values become zero or negative; the MW value calculation by LS/RI is not even possible. For these reasons, the M_z and M_{z+1} calculations of conventional GPC-LS method are even less precise than the conventional GPC using only the RI signal.

3.2. Theory

The new GPC-LS method we propose involves a simple change of computational algorithm and requires no change in the GPC-LS experiment. The change is to use the LS signals (instead of the RI signals) to couple with the conventional GPC-MW calibration curve to calculate sample MW. This approach takes advantage of the high-MW sensitivity of LS, but avoids the noise problem of the LS/RI ratio. It allows all materials detectable by LS be counted in the MW-average calculations even when RI signal is no longer detectable at the high-MW regions. The contrast of this new GPC-LS approach against the conventional GPC is illustrated in Fig. 2, again using the same HDPE data as in the earlier example for the polymer M_z calculation. The rational for the formulations needed for this new GPC-LS approach is explained in the following, again using the M_z calculation as an example.

3.2.1. Conventional GPC using only an RI detector (see Fig. 2)

$$\mathrm{RI}_i \approx w_i$$

$$M_z \equiv \frac{\sum w_i \times M_i^2}{\sum w_i \times M_i} = \frac{\sum \mathrm{RI}_i \times M_i^2}{\sum \mathrm{RI}_i \times M_i} \tag{2}$$

where RI_i is RI signal at GPC slice i, and M_i is the MW value at GPC slice i, taken from a conventional GPC-MW calibration curve.

High Order MW-averages by GPC-LS: A Link to Polymer Rheology

- **From RI Chromatogram Using Conventional GPC Calibration Curve: (Same Chromatogram, 4 different baseline & Integration Settings)**

$$M_Z = \frac{\sum w_i * M_i^2}{\sum w_i * M_i} = \frac{\sum RI_i * M_i^2}{\sum RI_i * M_i}$$

HiDPE					STD Dev	RSD
Mw	169,000	181,637	175,534	176,148	*7,086*	***4.09%***
Mz	847,096	1,352,729	996,058	1,018,472	*309,198*	***32.95%***
Mz+1	2,242,600	5,672,868	2,865,181	2,945,742	*1,627,723*	***54.68%***

- **From LS Chromatogram Using Conventional GPC Calibration Curve:**

$$M_Z = \frac{\sum w_i * M_i^2}{\sum w_i * M_i} = \frac{\sum RI_i * M_i^2}{\sum RI_i * M_i} = \frac{\sum (RI_i * M_i) * M_i}{\sum (RI_i * M_i)} = \frac{\sum LS_i * M_i}{\sum LS_i}$$

HiDPE					STD Dev	RSD
Mw	169,687	170,239	168,538	168,211	*1,202*	***0.52%***
Mz	837,058	852,146	844,633	841,895	*8,940*	***1.05%***
Mz+1	2,313,683	2,445,354	2,208,454	2,213,394	*99,146*	***4.34%***

Fig. 3. New high precision GPC-LS method against baseline setting variations.

3.2.2. Conventional GPC-LS calculation (see Fig. 2, equations not shown)

Since RI signal is proportional to sample weight concentration, and LS is proportional to both sample weight concentration and polymer MW at every GPC slice, we have

$$\mathrm{LS}_i \approx w_i \times M_i \approx \mathrm{RI}_i \times M_i$$

$$M_i \approx \frac{\mathrm{LS}_i}{\mathrm{RI}_i} \tag{3}$$

$$M_z \equiv \frac{\sum w_i \times M_i^2}{\sum w_i \times M_i} = \frac{\sum \mathrm{RI}_i \times M_i^2}{\sum \mathrm{RI}_i \times M_i} \tag{4}$$

where M_i in Eq. (4) is calculated as the ratio of LS/RI, from Eq. (3) for every GPC slice *i*. This way of calculating M_i has very poor precision when the RI signal becomes very weak in the high-MW region of the GPC elution curve.

3.2.3. The proposed new GPC-LS approach (see Fig. 2)

Since the LS signal is proportional to both sample weight concentration and the polymer MW at every GPC slice, we have

$$\mathrm{LS}_i \approx w_i \times M_i$$

$$M_z \equiv \frac{\sum w_i \times M_i^2}{\sum w_i \times M_i} = \frac{\sum \mathrm{LS}_i \times M_i}{\sum \mathrm{LS}_i} \tag{5}$$

$$M_{z+1} \equiv \frac{\sum w_i \times M_i^3}{\sum w_i \times M_i^2} = \frac{\sum \mathrm{LS}_i \times M_i^2}{\sum \mathrm{LS}_i \times M_i} \tag{6}$$

where LS_i is the light scattering signal at GPC slice *i*, and, M_i is the MW value at GPC slice *i*, with M_i taken from the conventional GPC-MW calibration curve.

Note that the M_z and M_{z+1} calculations according to Eqs. (5) and (6) use only the GPC-LS elution curve. No RI signal is used in the calculation. This is the way to avoid the problem in conventional GPC-LS method when the RI signal diminishes at the high-MW tail of the GPC elution profile.

3.2.4. Precision tests

Two tests are performed to demonstrate the improved precision of the new GPC-LS approach over the conventional GPC method:

1. The same GPC elution curve of an HDPE sample was reprocessed four times with some slight intentional variations in baseline and integration settings to simulate the usual operator errors. The variation of the calculated M_w, M_z, and M_{z+1} values from the two methods are compared in Fig. 3. The improvement of the precision of the new method over conventional GPC is quite drastic. The M_z values from the new GPC-LS calculation show a

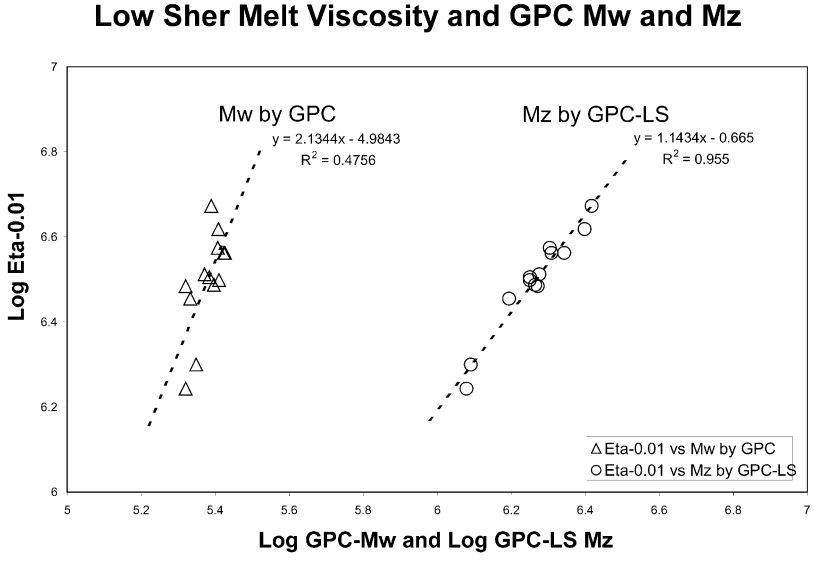

Fig. 4. Improved GPC-LS M_z correlation with low-shear melt viscosity.

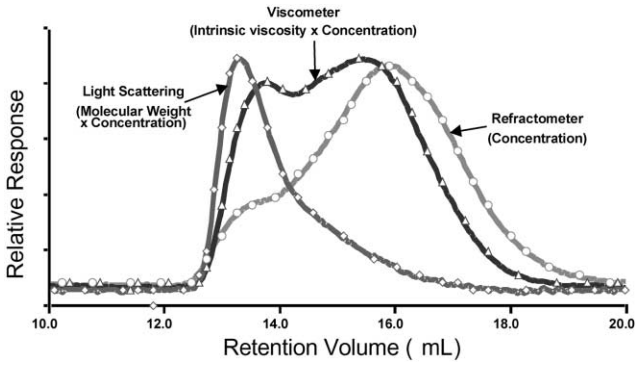

Fig. 5. 3D-GPC response for LDPE.

precision that is even better than that of the M_w values of the conventional GPC calculation.

2. Thirteen high-MW HDPE samples were run on the 3D-GPC system. The M_z values calculated from conventional GPC method using an RI detector are compared with the M_z values calculated from the new GPC-LS approach in Fig. 4. Again, we see the improved precision of M_z from the new method over the M_w of the conventional GPC. There is also a better correlation between the GPC-LS M_z values when plotted against the low-shear melt viscosity values, where the $\eta(0.01)$ data are the melt viscosity values taken at 0.01 per second shear rate.

3.2.5. Discussions

(1) The proposed GPC-LS method is intended to give improved precision of high-order MW averages for high-MW samples where the LS signal is significantly better than the RI signal. For polymer M_n values, the conventional RI-GPC calculation will invariably have better precision than the GPC-LS calculation. There could be no advantage of using GPC-LS method for samples of low MW that has poor LS signals.

(2) Since conventional GPC-MW calibration is based on standards of linear polymers, it means that the proposed GPC-LS approach also has the assumption of linear polymers. Under such circumstances, the MW accuracy is maintained when applying this method for high-MW HDPE samples without LCB. For other high-MW samples, the method will still provide high level of precision in the M_z and M_{z+1} values for useful relative comparison purposes, but these values may not be equal to the true MW values in the absolute sense.

(3) For high-MW HDPE samples like that of the pipe and HD film resins, the high precision advantage of this method proves to be very useful in solving industrial problems. For best results, it is highly desirable to use the low-angle LS capability of a PDI detector. As our interest is in large polymer structure, angular dissymmetry problem at large scattering angles can affect the MW calculation. The current work uses the 15° scattering channel of a PD2000 LS detector from Precision Detectors, Inc., 10 Forge Park, Franklin, MA 02038.

(4) Further precision improvement is still required for GPC-LS to provide results more meaningful in correlation with the rheology results. The remaining precision variance in this GPC-LS method is now resulting mainly from that of the conventional GPC-MW calibration curve. Instead of a single broad standard, our work is underway to use a bimodal broad standard to improve the calibration precision. This will further improve the overall precision of this new GPC-LS approach.

(5) The question of whether M_w in Eq. (1) is the right MW average to use to explain zero-shear melt viscosity relationship is of considerable interest for understanding polymer rheology. To study this, we want to examine MW averages other than the usual M_n, M_w, M_z, and M_{z+1} values. The following is a general formulation that can be used to calculate other MW averages based on the proposed GPC-LS method:

$$M_x = \left[\frac{\sum w_i \times M_i^x}{\sum w_i} \right]^{1/x} = \left[\frac{\sum \mathrm{LS}_i \times M_i^{(x-1)}}{\sum(\mathrm{LS}_i/M_i)} \right]^{1/x} \tag{7}$$

and for $x = 3.4$, we have

$$M_{3.4} = \left[\frac{\sum w_i \times M_i^{3.4}}{\sum w_i} \right]^{1/3.4} = \left[\frac{\sum \mathrm{LS}_i \times M_i^{2.4}}{\sum(\mathrm{LS}_i/M_i)} \right]^{1/3.4} \tag{8}$$

It would be interesting to see how the power law dependence of Eq. (1) might change when different MW average obtained at different x values is used to fit the rheology results.

4. The 3D-GPC technique and LCB determination

Fig. 5 shows an example of 3D-GPC separation for a low-density polyethylene (LDPE) sample. The molecules in this LDPE sample that are fractionated by the GPC column reach the three detectors to give three elution curves simultaneously. The refractometer (RI) signal is proportional to sample concentration, while the viscosity and LS detectors are also in proportion to the sample intrinsic viscosity, IV and MW, respectively. For this LDPE sample, the RI detects a small hump at the early eluting high-MW portion of the elution curve. The RI signal alone is not able to show whether or not this hump is consistent with the branching in the sample. However, near this early eluting hump, a large increase in LS is observed, while there is only a moderate increase in the viscosity DP signal. The relative intensity differences of these detector signals clearly indicate substantial LCB in the high-MW region of this sample [10].

The LCB distribution across polymer MWD can be studied from a M–H plot generated from the 3D-GPC results. The M–H plot is a log–log plot of polymer IV against MW across the GPC elution curve. The IV and

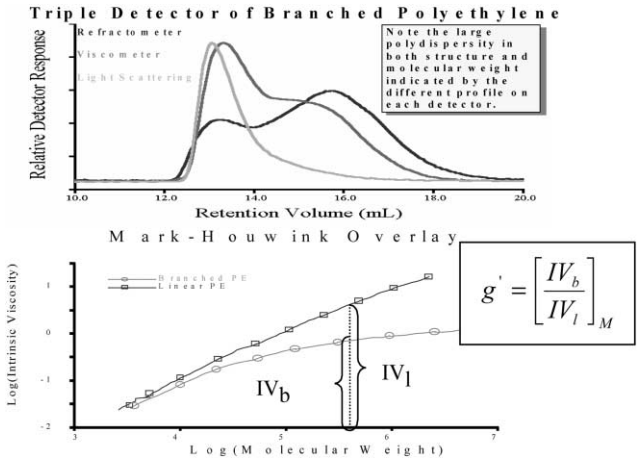

Fig. 6. M–H plot and LCB index by 3D-GPC.

MW value at every GPC slice is calculated by the ratio of experimental data DP/RI and LS/RI, respectively. A linear M–H plot of a slope of about 0.72 for a HDPE standard is used as reference to determine the LCB of LDPE samples. The M–H curve for an LDPE falls below this HDPE reference line because of the LCB in LDPE. Lower M–H curve means higher LCB. A GPC polymer LCB index g' can be calculated for every GPC-MW slice by using Eq. (9). This g' index is less than one for all samples containing LCB (see Fig. 6). This is because of the fact that for two molecules of same MW, the IV of the molecule with LCB will have to be lower than that of the linear molecule [10]:

$$g \equiv \text{GPC} - \text{LCB index} = \left[\frac{\text{IV}_\text{b}}{\text{IV}_\text{l}}\right]_\text{M} \tag{9}$$

Typical M–H plots obtained from 3D-GPC analyses can show subtle differences in the LCB features among different types of LDPE products. An example of this is shown in Fig. 7. The M–H plot of 3D-GPC can be a useful tool to solve various industrial problems. Fig. 8 shows an example where

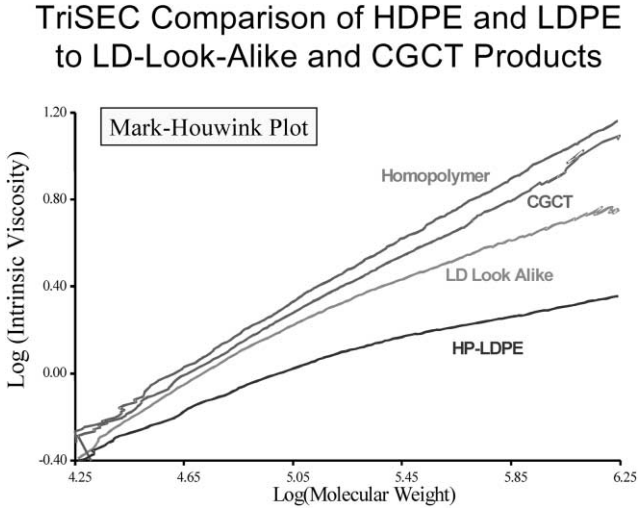

Fig. 7. LCB features of different LDPE resins.

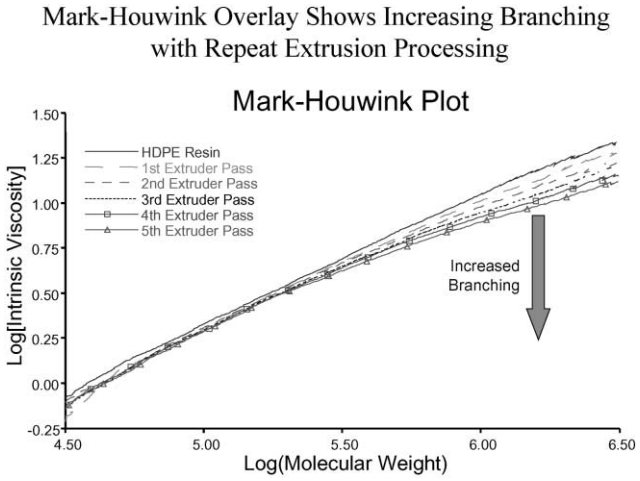

Fig. 8. Sensitive LCB detection in M–H plot of 3D-GPC.

the M–H plots from 3D-GPC are used in the detection of the onset of LCB and thermal degradation that occur during the extrusion process of pelletizing HDPE resins.

5. The 3D-TREF technique and SCB determination

5.1. The 3D-TREF instrument

Although 3D-GPC provides a useful tool for detecting LCB, but the technique is not sensitive to SCB. A more useful technique for SCB is the TREF technique [8,9]. The TREF technique relies on the crystallization and re-dissolution process to separate polymers having different levels of SCB. A 3D-TREF system encompasses three online detectors: infrared, IR; viscosity, DP; and light scattering, LS. Fig. 9 shows the components of an automated 3D-TREF system. The polymer sample dissolved in TCB is injected onto the TREF column at 150°C. The flow of TCB

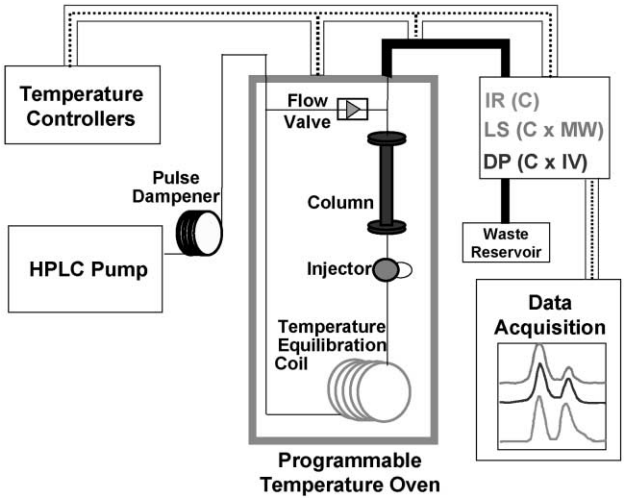

Fig. 9. Schematic of 3D-TREF system.

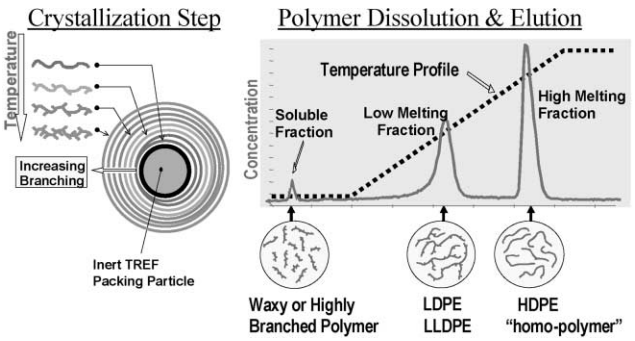

Fig. 10. TREF separation mechanism: crystallization and dissolution.

is then switch away from the column when the column is being slowly cooled down to 35°C. The TCB flow is then re-established through the TREF column, preparing the system for a controlled heating and elution step.

The crystallization step in Fig. 10 depicts the process where polymer fractions with different levels of SCB precipitate and coat the TREF packings during the cooling cycle. Polymer fractions coat the packing particles in layers with the most highly branched fraction precipitating out last to form the outer layer. In this picture of an 'onion ring structure', the outer layer of higher SCB will elute first in the elution step of the TREF cycle. The polymer dissolution and elution step in Fig. 10 depicts the 3D-TREF elution profile of sample SCB distribution. The elution peak detected immediately after the solvent flow is switched back to the TREF column is caused by the soluble fraction in the sample. As the temperature increases with time during this TREF elution cycle, the more branched molecules elute first, then the ones with decreasing SCB, followed by the more linear 'homopolymer fractions'. Therefore, the crystallization and heating cycles act in synergy to the formation, then the separation of the polymer layers on the surface of the TREF packings. This 3D-TREF system can use its autosampler to make up to 16 unattended runs at the rate of six samples a day. Each sample cycle consists a 3-h cooling followed by an 1-h heating and elution.

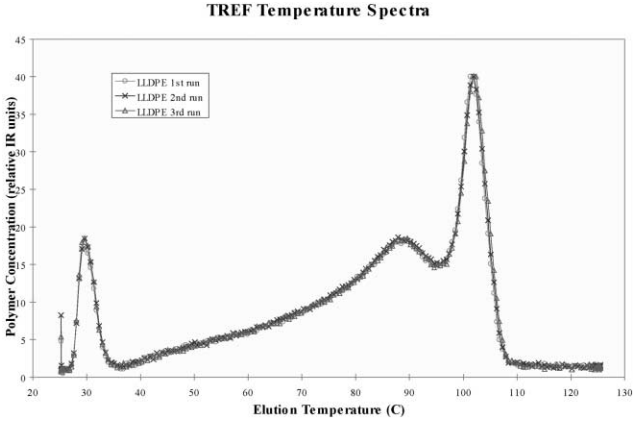

Fig. 11. Repeatability of automated TREF analyses.

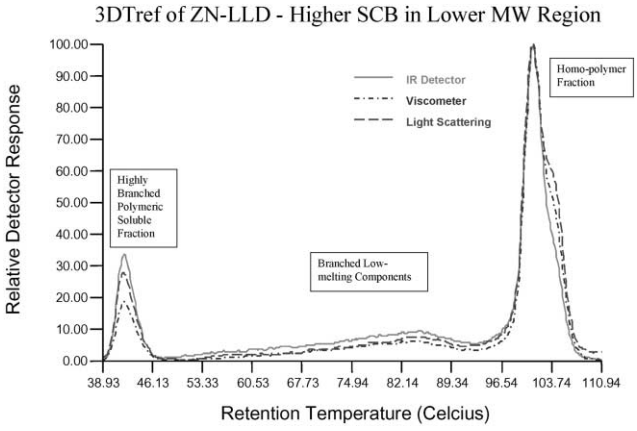

Fig. 12. 3D-TREF elution curve for a hexene ZN-LLDPE sample.

5.2. Repeatability of automated TREF analyses

A typical TREF curve for a Ziegler–Natta (ZN) LLDPE sample is shown in Fig. 11. This chromatogram shows the presence of a soluble fraction peak followed by a broad peak of branched polymer fraction in the mid-temperature region. The high-melting 'homopolymer' fraction is eluted last at the highest elution temperature. The reproducibility of our TREF is quite good as shown in Fig. 11.

5.3. The 3D-TREF analyses of MW dependency of SCB distribution in LLDPE

The 3D-TREF chromatogram for a hexene ZN-LLDPE is shown in Fig. 12. From the relative peak height of the LS, viscosity and IR detector signals, we can learn more about the SCB features of this sample. First, we can tell that the soluble fraction in this sample is made up with the highly branched polymers, not low-MW wax or oligomers. This conclusion is reached because of the existence of the high LS and viscosity signal associated with this soluble material. Secondly, we can tell that the hexene co-monomers are more concentrated in the low-MW part of the polymer MWD. This conclusion is reached also by observing the relatively higher-LS signal in the high-melting homopolymer peak, in comparison to the lower-melting materials of higher SCB from more hexene incorporation.

A reverse MW-dependency on SCB distribution is seen in some metallocene-based LLDPE (mLLD) samples. An example of which is shown in Fig. 13. For this sample, we see a higher-LS signal for the more branched low-melting component. This clearly indicates that the hexene co-monomers are more concentrated in the higher-MW portion of the polymer MWD. In this sample, there is little soluble fraction of polymeric in nature, which is quite contrary to the ZN samples. These are the structural features that are considered highly desirable for polyethylene products of good optical and physical properties.

6. Synergism of GPC–TREF

There exists close synergism between GPC and TREF. This is much like the synergism that one finds between two most common laboratory tests: the density and melt-flow index (MI). In many ways, TREF is more related to density and product properties, while GPC is more related to MI and flow properties.

An example of a classical case of how TREF and GPC can compliment each other is shown in Fig. 14. The GPC data clearly shows that the metallocene LLD is narrower in MWD than the two ZN-LLD samples. The hexene and butene ZN-LLD samples have nearly identical GPC curves. This is the expected result for changing only the comonomer type. The small difference of two-carbon (butene) versus four-carbon (hexene) side chains at the 10–20% co-monomer level is not expected to cause an enough change in the hydrodynamic volume of the polymer molecules that is sufficient to affect GPC elution. The three samples however have very different TREF profiles. A single narrow TREF peak is seen for the narrow SCB distribution of the metallocene LLD sample because of its single-site catalyst technology. The hexene and butene ZN-LLD samples are now well differentiated in the TREF results. The TREF curves of the ZN-LLD samples show that there exist three populations of very different levels of SCB. Co-polymer composition in this ZN-LLD is shown to be very heterogeneous that results from catalyst having multiple active sites.

7. A hybrid 3D-GPC–TREF instrument

An experimental hybrid system is built by installing a TREF add-on oven compartment to an existing Waters 150C GPC system with a build-in RI detector. Three additional detectors are added to the system. These are Foxboro IR, Viscotek 150R viscometer, and PDI 15 and 90° dual-angle LS detector. The configuration of the instrument is described by the schematic in Fig. 15. The six-port valve in the system automatically switches the solvent flow through either the GPC columns or the TREF columns at several predetermined set times.

While the sample is loaded in the TREF column and is being cooled down in the add-on oven from 150 to 35°C during the crystallization step, the solvent flow is automatically switched into the GPC column to allow the GPC separation of the polymer sample to take place. The GPC run is complete at the end of the 3-h crystallization step. At that time, the solvent flow is switched again. This time, the flow is directed into the TREF column to flush out the polymer from the TREF column. During this 1-h TREF elution step, the TREF oven temperature is programmed to increase linearly from 35 back to 150°C. The TREF elution is complete at the end this heating period. In this process, both GPC and TREF runs are complete in every 4-h cycle. With the use of the auto-sampler capability of the Waters 150C GPC system, up to 16 samples can be loaded at one time and analyzed in an unattended operation, at the rate of six samples for every 24 h. Fig. 16 shows an example of a hybrid GPC–TREF run on a hexene ZN-LLD polyethylene sample. The temperature profile during the cooling and the heating cycle is also recorded as shown in Fig. 16.

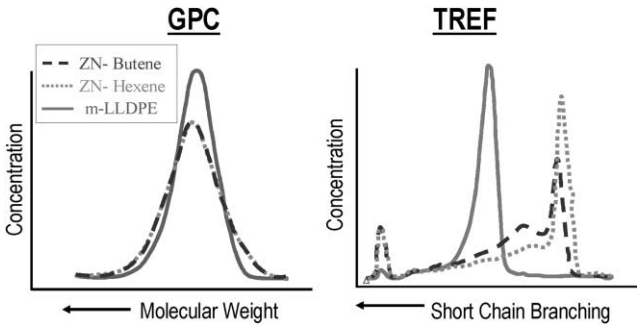

Fig. 14. Comparison of LLDPE types by GPC and TREF.

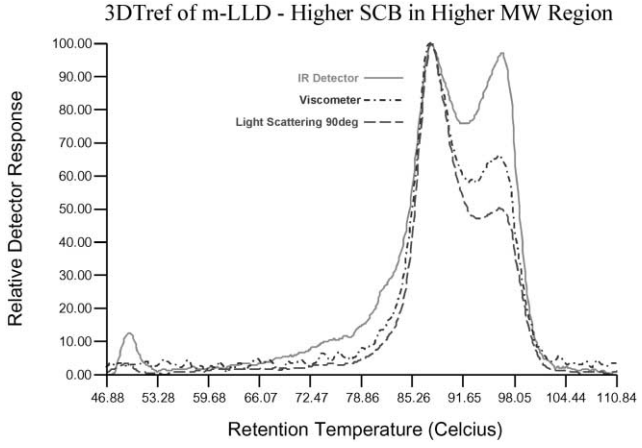

Fig. 13. 3D-TREF elution curve for a hexene m-LLDPE sample.

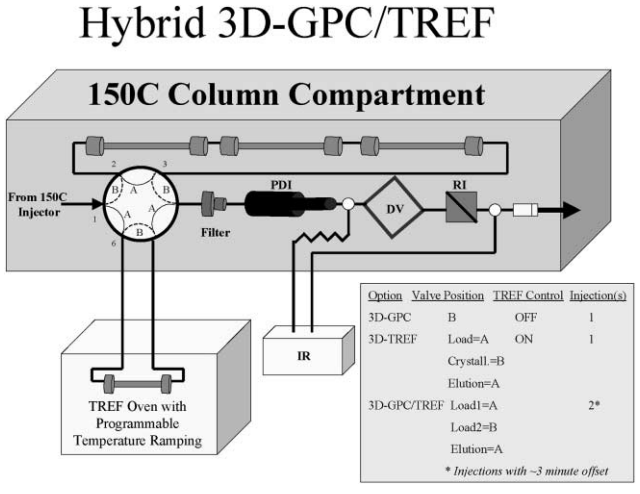

Fig. 15. Configuration of the hybrid 3D-GPC–TREF system.

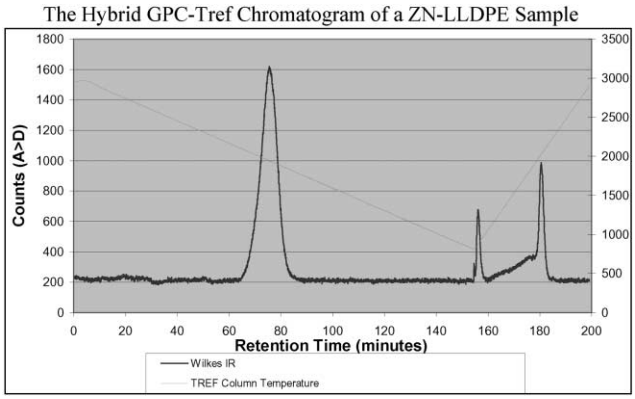

Fig. 16. The hybrid GPC–TREF chromatogram of a hexene ZN-LLDPE.

8. Polymer microstructure plot (3D-GPC and 3D-TREF combined)

There is a wealth of polymer structural information in the combination of 3D-TREF and 3D-GPC results. A polymer microstructure plot is created which consists of sample comparative overlay curves of both 3D-GPC and 3D-TREF results in one graphic display. An example of such a plot is shown in Fig. 17, which gives an in-depth comparison of the microstructure differences between two LDPE samples. This overlay approach of using all six detector signals provides a very effective tool for detecting subtle differences between good and bad resin lots or for comparing competitor's resins. They are useful for fine-tuning and optimizing resin designs for specific applications, either by blending or changing catalysts and reactor conditions. The detailed molecular architectures displayed by this polymer microstructure plot are very useful to study the products made from the new controlled geometry catalyst technologies (CGCT) and the low-density look-alike products.

The information in some parts of the microstructure plot might be more important than the other parts, and situation could vary depending on the particular interests of each individual resin study. A proper balance of interpreting the information needs to consider the purpose of each specific resin application. It is helpful however to mention a few useful general tips in interpreting the microstructure results, as shown for example in Fig. 17. The arrows marked on the plot in Fig. 17 illustrate the trend of changing LCB, MI, MW, molecular size, SCB or density, with respect to the 3D-GPC and 3D-TREF measurable. For the two LDPE samples in this figure for example, the LS detector in the 3D-GPC part of the plot clearly shows that there is much more LCB for the sample labeled as LDPE-1. On the other hand, the 3D-TREF part of the plot shows that the co-monomer incorporation is narrowly distributed in both these LDPE samples. The sample labeled LDPE-1 has much more co-monomer (lower elution temperature) than the LDPE-2 (NBS 1476) sample. With practice, a 'snapshot' view of the microstructure plot can give a considerable appreciation for the molecular architecture of any resin sample by applying these few simple rules mentioned above.

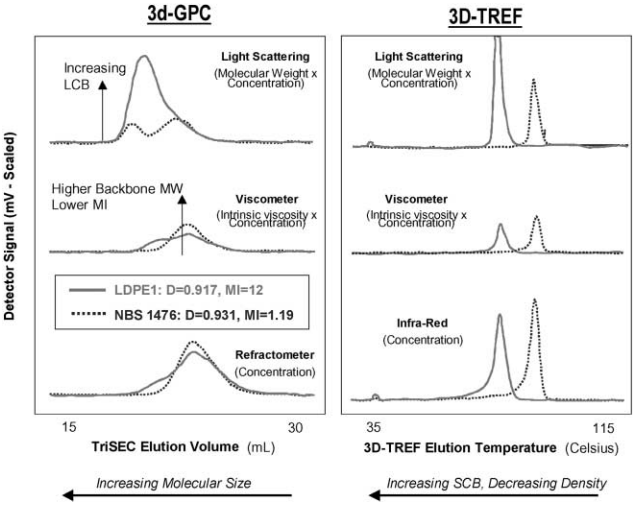

Fig. 17. Microstructure plot comparison of LDPE samples.

9. Polymer microstructure examples

9.1. Polymer blend composition study

The information shown by the microstructure plot is useful for optimizing polymer blend design in choosing the right resins of the desired polymer MW, MWD, SCB, and LCB distributions. One nice feature of TREF analysis is its ability to analyze the composition of polymer blends. The TREF curves of individual components in a blend can be added directly to make up the overall TREF curve for the blend. An example of this application is shown in Fig. 18 for a three-component blend of HD, LD and LLDPE resins in a film product. Using a deconvolution calculation, we can determine the weight composition of each component in the blend. As shown in the figure, the sum of the resin TREF curves with the appropriate weighting factors matched well with the experimental TREF curve of the film sample. The additive substances that are compounded into the blend during the film-fabrication process cause the size mismatch of the soluble fraction peak.

Fig. 19 shows another example. In this case, one of the company resins is used in a blend with an unknown resin to make a film product at a converter location. From the graphs shown in the plot, one can see that the other component used in the film is a HD resin. Furthermore, from the TREF peak area measurements, the actual blending ratio used in this film construction can be calculated. Using a numerical deconvolution process, one can also retrieve the MW and MWD information of this unknown HDPE component. The very noisy scattered TREF-LS signal on the film sample in Fig. 19 is very interesting. This situation in TREF is generally observed when there are color pigments or TiO_2 present

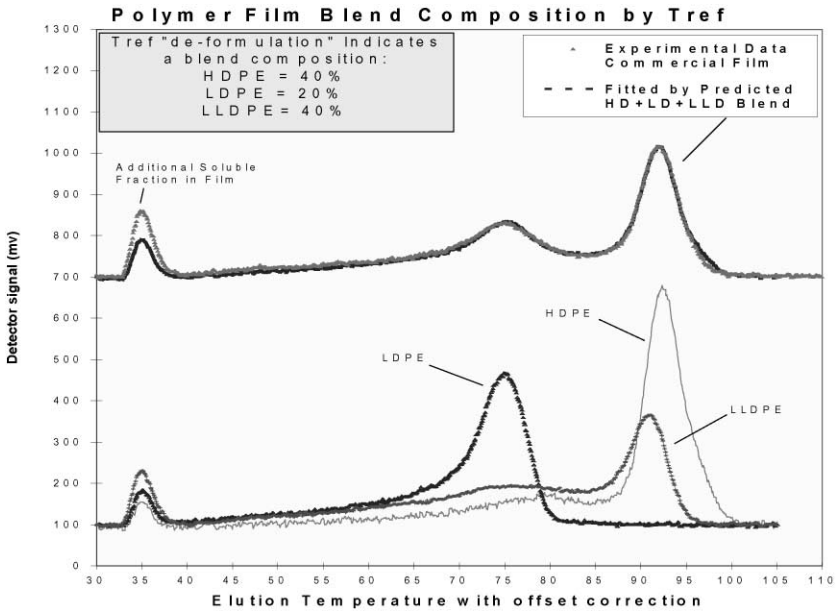

Fig. 18. TREF study of polymer film blend composition.

in a film sample. This result suggests that there is some polymer to pigment association, which by itself is an interesting phenomenon that requires further study.

9.2. Polymer microstructure of CGCT resin

In the example shown in Fig. 20, the microstructure of a CGCT resin is compared with a ZN-LLD resin. There are several points worth mentioning in these results. First, some LCB is apparent for the ZN-LLD sample from the 3D-GPC-LS curve. This is an unexpected finding. Long-chain branching is not commonly expected in ZN-LLD processes. It would be interesting to find out how and where the LCB is formed in the ZN process. The 3D-TREF curves show a soluble fraction in the sample that is polymeric in nature. The presence of a large amount of soluble polymeric material seems to be related to a film 'blockiness' problem of this resin.

Secondly, for the CGCT resin in Fig. 20, the 3D-GPC part of the plot shows that the sample has the narrow MWD. This is what one expects for a single-site metallocene product. The 3D-TREF curves of this CGCT sample are interesting. This sample has a very small soluble fraction peak. Its high-melting peak is much smaller and elutes much earlier at a

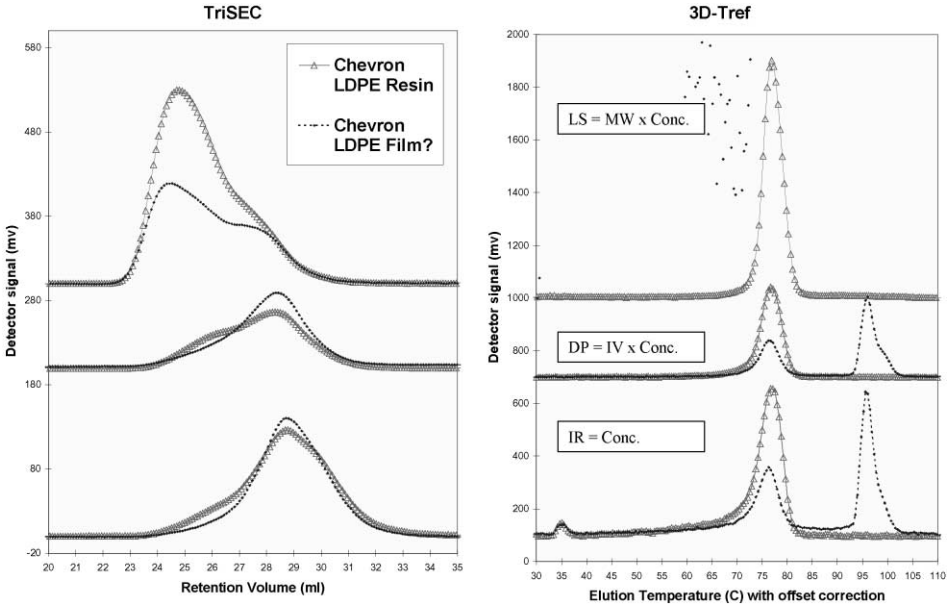

Fig. 19. Microstructure evaluation of post-fabrication film blend.

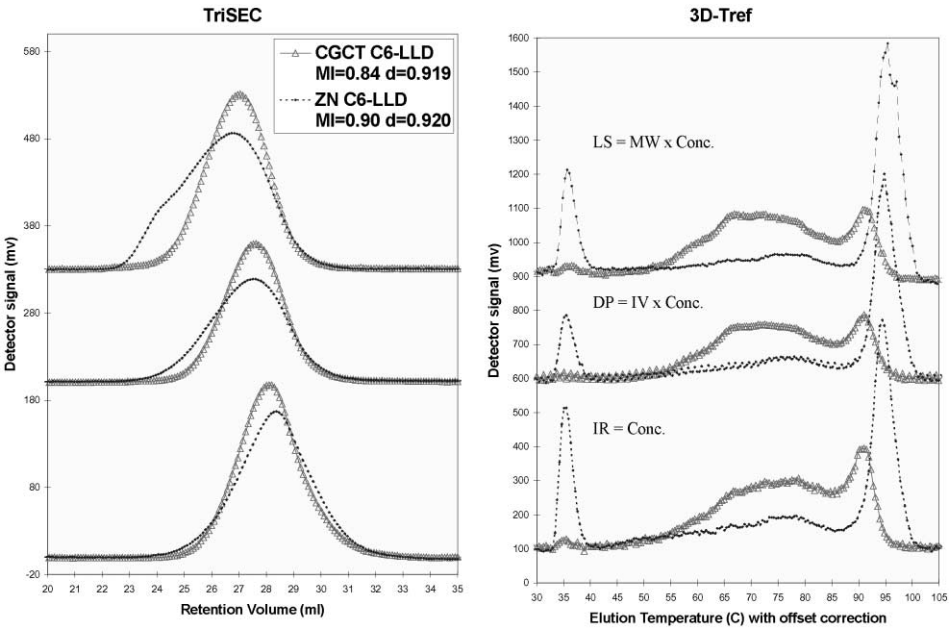

Fig. 20. Microstructure evaluation of ZN versus CGCT-LLDPE.

lower elution temperature than that of the ZN sample. These results suggest that the hexene incorporation to polymer is much more efficient in CGCT than in ZN. Another way of saying that is, in ZN, more hexene co-monomers are incorporated in the soluble-fraction population, while the higher-MW homopolymer fraction has stayed at high melting due to lack of co-monomer incorporation.

The fact that these two samples have nearly the same density value is worth noting. This implies that density is an average quantity of the bulk sample, and it is not capable of accounting for the large CCD and SCBD differences between these samples seen in this example. The much narrower CCD of the CGCT sample is obviously a very important quality of this product. Compared to ZN, it means better optics, better impact strength, better drawdown potential, and much lower film blockiness problems.

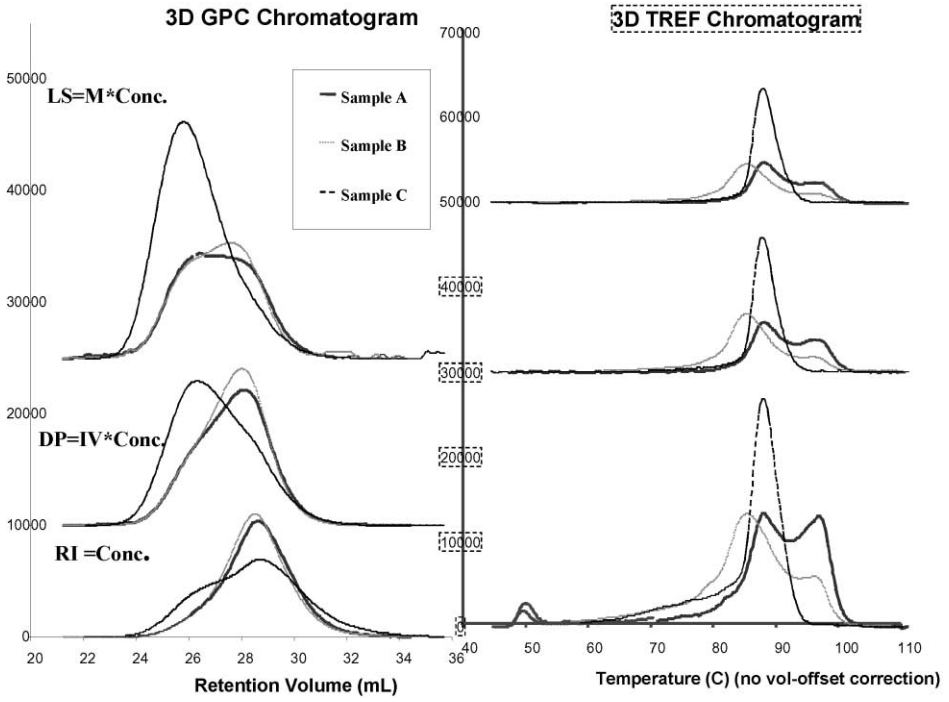

Fig. 21. Microstructure evaluation of novel resin structures.

There is one more observation that is important to this CGCT sample. By comparing the relative peak heights of this sample in the 3D-TREF profiles between the high-melting peak (85–95°C) and the broad peak in the middle (50–85°C), one sees that polymer in the broad peak has a higher viscosity and LS signal. This would indicate that the material covered under the broad middle peak, which is of higher-SCB content, has a higher-MW value than the material eluted in the higher-temperature peak of lower SCB content. This MW dependency of CGCT is directly opposite to that found in conventional ZN-LLD samples. These differences are highly relevant to the optical and physical properties of these two resins.

9.3. Catalyst reaction sites study

The polymer microstructure plot is very useful in supporting catalyst research and product development efforts, as shown in the example in Fig. 21. In this figure, a comparison is made on three polymer resins made under various catalyst conditions and reaction kinetics. There are numerous interesting differences in these resins seen by the 3D-GPC–TREF techniques. We can see that there are single-site versus multiple-site catalyst differences. There are LCB, SCB and MWD differences as well. Viewing the resin structures through these overlay plots makes it easy to track the trends of experimental results of reactor trials, and helps to shorten the product development cycle time.

10. Conclusions

We find that the combination of 3D-GPC and 3D-TREF forms a pair of valuable analytical tools that complement each other well in studying many areas of polymer interests where the understanding of polymer structure–property relationships is of central importance. Not only is the combination of these two techniques useful in understanding the desired microstructure for a given resin, the combination of the techniques finds great utility in analyzing blended components.

Moreover, the power to simultaneously view CCD and MWD yields a snapshot into resin microstructure without processing the data in a numerical manner. When processed numerically, absolute molecular weight and MWD can be determined, LCB can be quantified with Zimm–Stockmayer theory, and SCB distribution can be obtained by calibrating the TREF temperature dependence with a series of narrow CCD standards.

Acknowledgements

The authors wish to thank Rod Byerly, Tod Gipson, John Talbert and Linda Nemcheck for obtaining much of the experimental results presented in this presentation. The authors wish to thank Fred Noyes and Porter Shannon for providing the low-shear melt viscosity data obtained on a Rheometrics ARES parallel plate rheometer.

References

[1] Fawcett EW, Gibson RO, Perrin MW, Patton JG, Williams EG, B Patent 471,590, September 6, 1937.
[2] Ziegler K. Ger Patent 878,560, 1953.
[3] Boor J. Ziegler–Natta catalysts and polymerizations. New York: Academic Press, 1979.
[4] McDaniel MP, Johnson MM. Macromolecules 1987;20:773.
[5] Kaminsky W. Macromol Chem Phys 1996;197:3907.
[6] Lai S, Knight GW. RETEC 1993.
[7] Yau WW, Kirkland JJ, Bly DD. Modern size exclusion liquid chromatography. New York: Wiley, 1979.
[8] Wild L. Adv Polym Sci 1991;98:1–47.
[9] Soares JBP, Hamielec AE. Macromol Theory Simul 1995;4:305.
[10] Haney MA, Gillespie D, Yau WW. Today's Chemist 1994;3(11):39.
[11] Lecacheux D, Lesec J, Quivron C. J Appl Polym Sci 1982;27:4867.
[12] Yau WW, Gillespie D. An automated triple-detector TREF instrument for polyolefin research. Waters 98 International GPC Symposium Volume, October 1998.
[13] Tuminello WH. Relating rheology to molecular weight properties of polymers, Polymer proceedings and flow dynamics, Encyclopaedia of fluid mechanics, vol. 9. Gulf Publications, 1989.
[14] Mavridis H, Shroff RJ. Appl Polym Sci 1993;49:299–318.
[15] Wasserman SH, Graessley WW. Polym Engng Sci 1996;36:852–61.